Journal of Applied Physics

RESEARCH ARTICLE | APRIL 15 2025

Heterogeneous domain structure induced by alternating current poling in $Pb(Mg_{1/3}Nb_{2/3})O_3$–$PbTiO_3$ single crystal

Woo-Jin Choi ; Hye-Lim Yu ; Jeong-Woo Sun ; Sang-Goo Lee ; Yoon-Sang Jeong; Wook Jo

Check for updates

J. Appl. Phys. 137, 154101 (2025)
https://doi.org/10.1063/5.0260627

View Online Export Citation

Articles You May Be Interested In

In vitro and *in vivo* high-frequency ultrasound response of microbubbles

J. Acoust. Soc. Am. (May 2006)

Towards the modeling of high-frequency ultrasound scattering from cells

J. Acoust. Soc. Am. (May 2008)

Achieving high piezoelectric performance in $Pb(Mg_{1/3}Nb_{2/3})O_3$–$PbTiO_3$ ferroelectric single crystals through pulse poling technique

J. Appl. Phys. (October 2024)

15 May 2025 04:16:25

AIP Publishing

Journal of Applied Physics

Special Topics Open for Submissions

Learn More

AIP Publishing

Journal of Applied Physics ARTICLE pubs.aip.org/aip/jap

Heterogeneous domain structure induced by alternating current poling in $Pb(Mg_{1/3}Nb_{2/3})O_3$–$PbTiO_3$ single crystal

Cite as: J. Appl. Phys. **137**, 154101 (2025); doi: 10.1063/5.0260627
Submitted: 25 January 2025 · Accepted: 26 March 2025 ·
Published Online: 15 April 2025

View Online Export Citation CrossMark

Woo-Jin Choi,[1] Hye-Lim Yu,[1] Jeong-Woo Sun,[1] Sang-Goo Lee,[2] Yoon-Sang Jeong,[2] and Wook Jo[1,a)]

AFFILIATIONS

[1]School of Materials Science and Engineering, Ulsan National Institute of Science and Technology, 50 UNIST-gil, Ulsan 689-798, Republic of Korea
[2]iBULe Photonics, Inc., 7-39, Songdo-dong, Yeonsu-gu, Incheon 21999, Republic of Korea

[a)]**Author to whom correspondence should be addressed:** wookjo@unist.ac.kr.

ABSTRACT

The thickness of the piezoelectric single crystals is known to have a significant impact on their piezoelectric properties. For high-performance transducers used in high-frequency medical diagnostic applications, the thickness of the piezoelectric single crystals must be reduced. However, the scaling effect, where the piezoelectric and dielectric properties deteriorate as the thickness decreases, remains insufficiently understood, and the mechanisms underlying this phenomenon are unclear. To address this issue, we investigated the changes in polarization and dielectric properties and the underlying mechanism of the scaling effect in alternating current (AC)-poled rhombohedral [001]-oriented $0.72Pb(Mg_{1/3}Nb_{2/3})O_3$–$0.28PbTiO_3$ (PMN–28PT) single crystals with respect to the sample thickness. The typical scaling effects, commonly observed with decreasing sample thickness, were confirmed through the degradations in polarization and dielectric properties of AC-poled crystals. The AC-poled crystals exhibited 109.5° domain walls parallel to the (001) plane, and the domain sizes in the surface layer were more than double those in the inner region regardless of thickness. The larger domain size in the surface layer reduces the density of the relatively soft 109.5° domain boundaries, thereby it causes an increase in the coercive field and degradation of the dielectric properties as the thickness decreases. The accumulated space charge on the surface induced an internal bias field for the thin samples, which is considered the origin of the large 109.5° domain size in the surface layer by applying the clamping pressure on the domains within that layer. This unexplored mechanism could contribute to solving the scaling effect problem in PMN–28PT single crystals for high-frequency ultrasound biomicroscope applications.

© 2025 Author(s). All article content, except where otherwise noted, is licensed under a Creative Commons Attribution-NonCommercial 4.0 International (CC BY-NC) license (https://creativecommons.org/licenses/by-nc/4.0/). https://doi.org/10.1063/5.0260627

15 May 2025 04:16:25

INTRODUCTION

Piezoelectric materials, which enable the interconversion between mechanical and electrical energy, have been widely used in electromechanical devices such as actuators and transducers.[1,2] Ferroelectric binary solid solution $(1-x)Pb(Mg_{1/3}Nb_{2/3})O_3$–$xPbTiO_3$ (PMN–PT) single crystals oriented along the [001] direction have attracted significant attention not only from industry but also from research field due to their excellent piezoelectric coefficients ($d_{33} > 1500$ pC/N), electromechanical coupling coefficients ($k_{33} > 0.90$), and high free dielectric permittivity ($\varepsilon_{33}^T/\varepsilon_0 > 5000$), which outperform those of commercialized $PbZr_{1-x}Ti_xO_3$ (PZT) ceramics.[3–6] Ferroelectric crystals should be electrically polarized to activate their piezoelectricity. Various post-treatment methods, such as field-cooling poling,[7–9] corona poling,[10–12] and stress assisted electrical poling,[13,14] etc., have been proposed as an effective approach to induce piezoelectricity and enhance the piezoelectric properties through domain engineering. The alternating current poling (AC-poling) method has recently been proposed as a simple and cost-effective substitute for the direct current poling (DC-poling) method, improving both the dielectric and piezoelectric properties of [001]-oriented relaxor–PT single crystals.[15,16] Using [001]-oriented relaxor–PT single crystals with an AC-poling

© Author(s) 2025

technique represents a promising strategy to enhance the sensitivity and expand the frequency bandwidth of ultrasound-based piezoelectric transducers for medical diagnostic applications.[17–20]

Ultrasound biomicroscopes utilizing piezoelectric materials have been of interest for applications such as the diagnosis of ocular lesions, cardiovascular diseases, etc.[20–22] Higher center resonance frequency and wider bandwidth have been in demand to achieve better axial resolution and sensitivity of the transducers.[19,20,23] For example, the operational frequency of transducers used for intravascular and ocular ultrasound imaging generally ranges from 20 to 60 MHz[22] and 35 to 50 MHz,[21] respectively. The frequency constant N_t is expressed as $N_t = f_r \times t$, where f_r is the resonance frequency and t is the thickness along the vibration direction.[24] The [001]-oriented relaxor–PT single crystals exhibit a lower frequency constant (N_t) compared to PZT ceramics due to their relatively high elastic compliance (s_{33}^E), which results in a decrease in their resonance frequency, following the relationship $f_r \propto \sqrt{\frac{1}{s_{33}^E}}$.[25–27] For high-frequency ultrasound diagnosis applications with high performance, the single crystals may need to be thinner than PZT ceramics to achieve the same resonance frequency due to their lower frequency constant (N_t).[25–27] However, it has been reported that the dielectric and piezoelectric properties decrease as the sample thickness decreases for piezoelectric ceramics and single crystals, so-called the scaling effect.[27–38] Several mechanisms to account for this phenomenon have been suggested, such as surface residual stress,[27,28,31,32,38] interface effect,[31] and domain size effect.[29,30,36] Namba *et al.*[27] recently observed the mechanically damaged domain structure in the surface layers of DC-poled PMN–PT single crystals, caused by the grinding process. They argued that the damaged surface layer, which could be removed through thermal annealing, hinders polarization rotation.[26] Li *et al.*[31] claimed that the thickness-dependent dielectric permittivity ($\varepsilon_{33}^T/\varepsilon_0$) of Mn-doped PMN–PT crystals can be attributed to surface residual stress and interface clamping effects, both of which may suppress polarization switching or vibration. Lee *et al.*[29,30] suggested that the scaling effect on the dielectric permittivity ($\varepsilon_{33}^T/\varepsilon_0$) and electromechanical coupling factor (k_{33}) might be caused by disruption of the equilibrium 4R domain structures and limited polarization rotation as the thickness of [001] DC-poled rhombohedral piezoelectric crystals approaches their domain size. It has been reported that the AC-poled [001]-oriented relaxor–PT crystals also exhibit the scaling effect due to their mechanically damaged and rough surfaces.[33,34,36,37] It was reported that surface residual stress altered the dielectric properties of crystals, which leads to noticeable differences in the dielectric permittivity above T_m, depending on its surface conditions (such as degree of roughness, annealing, etching, etc.) or sample thickness.[31,34] However, other studies have shown that the dielectric permittivity above T_m converges irrespective of the sample thickness.[29,30,35,37] This indicates that the scaling effect mechanism in these cases is only valid when the material is in the ferroelectric phase, which has domain structures with spontaneous polarization. In light of previous studies, the domain structure of the [001]-oriented relaxor–PT single crystals may contribute to the scaling effect. Although numerous studies have been conducted on the thickness-dependent domain size in ferroelectric materials, little has addressed the changes in the domain structure of the AC-poled [001]-oriented relaxor–PT single crystals depending on the sample thickness, and the issue remains unclear. Therefore, research on the scaling effect related to the domain structure of AC-poled [001]-oriented relaxor–PT is essential for achieving high performance in high-frequency ultrasound transducer applications.

We propose an unexplored mechanism underlying the scaling effect in AC-poled [001]-oriented rhombohedral PMN–28PT single crystals. Prior to measurements, the tailored crystals were annealed above 600 °C to eliminate dicing and polishing-induced surface residual stress. It was found that the domain structure of AC-poled crystals consisted of 109.5° domain wall parallels to the (001) plane, and the domain size in the surface layer was more than twice that of the inner region regardless of the sample thickness. It indicates that the density of 109.5° domain wall, which is more piezoelectric active (i.e., softer) than 70.5° domain wall, decreased with decreasing sample thickness due to the increased volume fraction of the surface layer. As a result, the coercive field (E_c) increased, while both the remnant polarization (P_r) and dielectric properties degraded as the sample thickness decreased. Therefore, the scaling effect can be caused by the large domain size in the surface layer in AC-poled [001]-oriented PMN–PT single crystals. It was observed that the internal bias (E_i) gradually shifted toward more negative values as the sample thickness decreased. The large domain size in the surface layer may be stabilized by clamping pressure from the accumulated space charge, which moves readily during the first half of the AC cycle but becomes trapped during the subsequent AC-poling cycles.

MATERIALS AND METHODS

PMN–28PT single crystals were grown along the crystallographic [001] direction using the vertical Bridgman method at iBULe Photonics Co., Ltd. (Incheon, Republic of Korea). The single crystal samples were then diced into $5 \times 5\ mm^2$ squares with thicknesses of 1000, 500, 250, 125, and 100 μm along the [001] direction, and their crystallographic orientations were confirmed using a real-time Laue system. The plate samples were heated above 600 °C in a furnace to eliminate surface residual stress induced during the dicing process. Gold electrodes were vacuum-sputtered onto both sides of the (001) plane surface of the single crystal samples to measure their electrical properties.

The single crystal samples were heated at 300 °C with short-circuited electrodes to achieve a fully depolarized state before the experiments. The dielectric properties of samples were measured at room temperature with an impedance-phase gain analyzer (HP 4194a, Hewlett-Packard, Palo Alto, CA, USA). For the alternating current (AC) poling process and electric field-dependent polarization measurements, a bipolar triangular with a peak-to-peak electric field of 10 kV/cm at 1 Hz was applied using the TF analyzer 3000 (aixACCT, Germany). The poled single crystal samples were fractured, and then the Pt electrode was deposited onto the freshly cleaved surface using an ion sputter (E-1045, Hitachi High-Technologies Corp. Japan). The domain structures of single crystal samples were then observed through the cleaved surfaces using a scanning electron microscope (SEM) (Quanta-200, FEI Co., Hillsboro, Oregon, USA). The domain size and surface layer were then analyzed using ImageJ software (LOCL, University of Wisconsin, USA).

15 May 2025 04:16:25

© Author(s) 2025

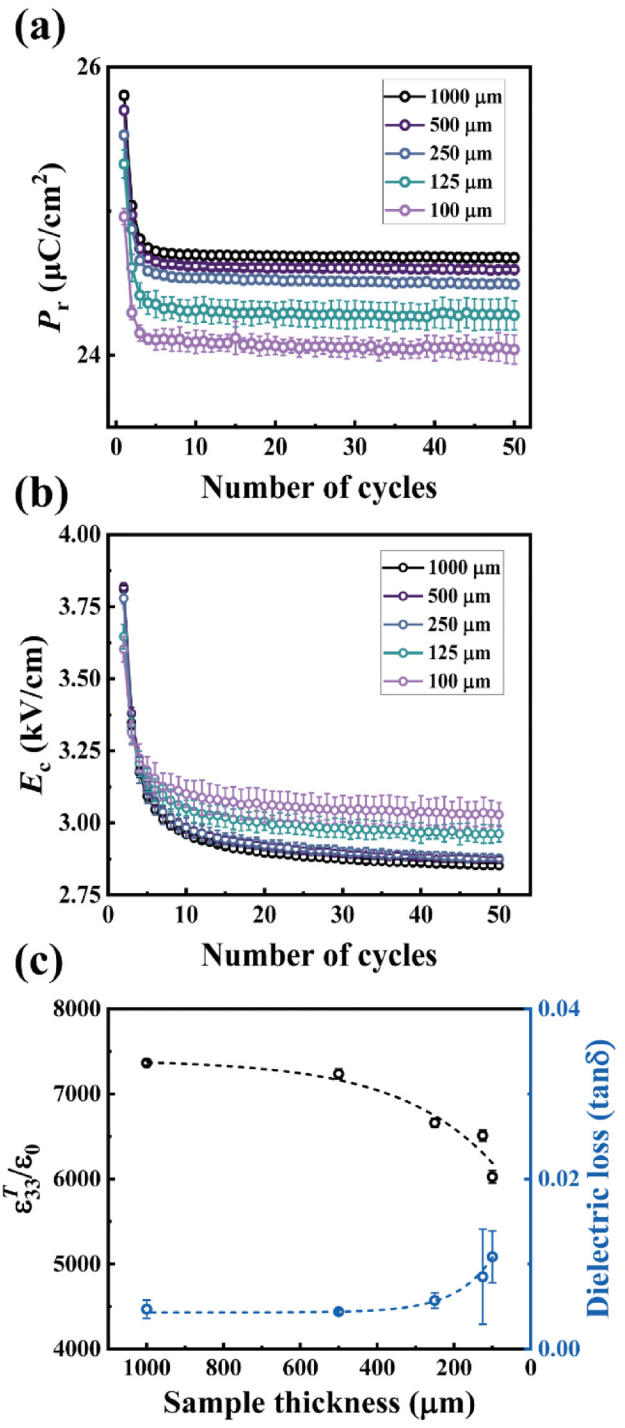

FIG. 1. (a) Remnant polarization (P_r), (b) coercive field (E_c) measured from the electric field-dependent polarization curves as a function of the number of AC-poling cycles, and (c) free dielectric permittivity ($\varepsilon_{33}^T/\varepsilon_0$) and dielectric loss (tanδ) at 1 kHz of AC-poled (50 cycles) PMN–28PT single crystal samples with varying thicknesses of 1000, 500, 250, 125, and 100 μm.

RESULTS AND DISCUSSION

Figures 1(a) and 1(b) show the remnant polarization (P_r) and coercive field (E_c) of the PMN–28PT single crystal samples measured from the P–E hysteresis loops (see Fig. S1 in the supplementary material) as a function of the number of AC-poling cycles (N_c) for different sample thicknesses. Both P_r and E_c rapidly decreased during the first five cycles and then plateaued as the number of AC-poling cycles (N_c) increased regardless of sample thickness. After the fifth cycle, the saturated P_r decreased, whereas the saturated E_c increased as the sample thickness decreased. The free dielectric permittivity ($\varepsilon_{33}^T/\varepsilon_0$) decreased, while the dielectric loss (tanδ) increased gradually with decreasing sample thickness measured at 1 kHz as shown in Fig. 1(c). Budimir *et al.*[39–41] investigated how the Gibbs free energy of the ferroelectric perovskite materials changes as a function of polarization to understand the mechanism enhancing piezoelectric properties within the framework of the Landau–Ginzburg-Devonshire theory. They argued that the degree of flatness in the Gibbs free-energy landscape, given external conditions such as temperature, pressure, etc., determines the dielectric susceptibility and piezoelectric response.[41] The domain walls in ferroelectric perovskite materials induce electric and stress fields in regions adjacent to the domains in contact, leading to modifications in both their dielectric and piezoelectric properties.[42] It is well known that the 109.5° and 70.5° ferroelastic domain walls can exist in the rhombohedral phase PMN–PT.[43–45] Wang *et al.*[42] demonstrated that the 109.5° domain wall exhibits a flatter Gibbs free-energy landscape than that of the 70.5° domain wall in lead-based perovskite ferroelectrics. Therefore, domains adjacent to the 109.5° domain wall possess a soft path and exhibit soft piezoelectric features, e.g., high dielectric (ϵ_r) and piezoelectric (d_{33}) constants with a lower coercive field (E_c). In contrast, domains near the 70.5° domain wall have a hard path, which leads to depressed piezoelectric properties and a higher coercive field. In addition, the polarization vector of domains adjacent domain walls is closer to the [001] direction than that of domains with spontaneous polarization oriented along the [111] direction, oriented at 54.7° from [001] in the rhombohedral phase PMN–PT single crystal.[46] Wan *et al.*[45] observed that the 70.5° domain walls rapidly decreased during the initial stage of AC-poling, particularly within the first five cycles, while the 109.5° domain walls became dominant as the number of AC-poling cycles exceeded five. The domain structures of DC-poled and five cycles of AC-poled samples with a thickness of 1000 μm were observed as shown in Fig. S2 in the supplementary material. The herringbone-like domain structure, exhibiting the mixed 70.5° and 109.5° domain walls typical of the rhombohedral phase ferroelectrics, was observed in the DC-poled sample. In contrast, the 70.5° domain walls were significantly reduced, such that periodic 109.5° domain walls became more distinct after five cycles of AC-poling. It was confirmed that the thickness-independent decreases in both P_r and E_c during the first five cycles can be attributed to the reduced density of 70.5° domain walls. The thickness-dependent saturated P_r, E_c, and dielectric properties of AC-poled samples may arise from differences in the domain structure of AC-poled single crystals depending on sample thickness.

Figure 2 shows SEM images of the surface layer and inner region of the AC-poled PMN–28PT single crystal samples with thicknesses

15 May 2025 04:16:25

© Author(s) 2025

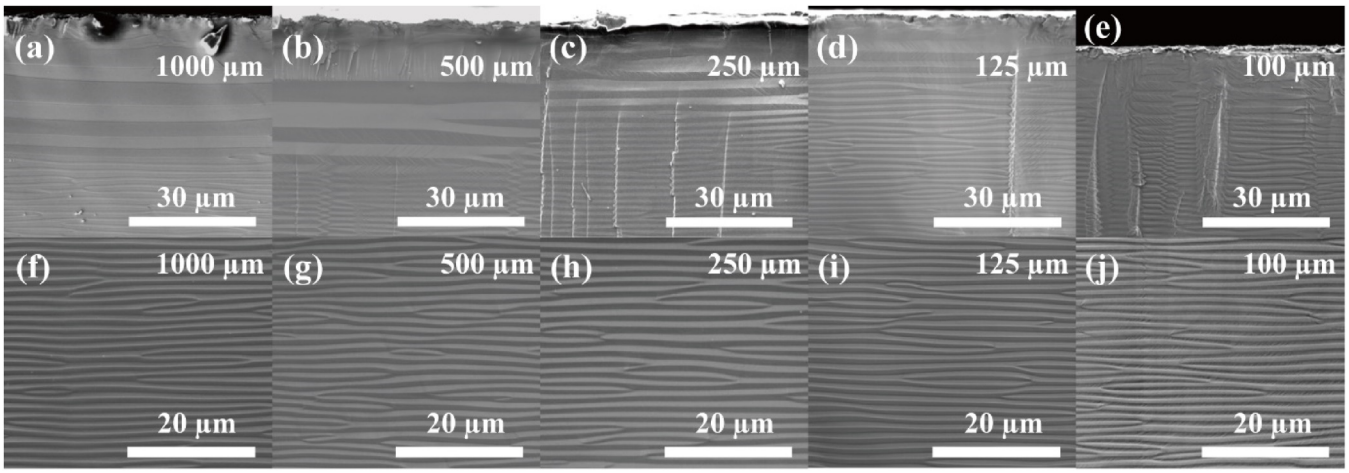

FIG. 2. Scanning electron micrographs of the surface layers (a)–(e) and inner regions (f)–(j) of PMN–28PT single crystal samples with thicknesses of 1000, 500, 250, 125, and 100 μm, respectively, after 50 cycles of AC-poling.

of 1000, 500, 250, 125, and 100 μm. The periodic 109.5° domains parallel to the (001) plane were observed regardless of sample thickness, as reported in previous studies.[45,47,48] It is noteworthy that the domain sizes were nearly identical in the inner regions, whereas larger domain sizes were observed in the surface layer.

The surface layer thickness, which consisted of larger domains, and the domain sizes in both the surface layer and the inner region of AC-poled PMN–28PT single crystal samples were measured by SEM image analysis as shown in Fig. 3 and Table I. The distribution of surface layer thickness and domain size in the surface layer is depicted in Fig. S3 in the supplementary material. The measured domain sizes in the inner region ranged from 0.66 to 0.74 μm and showed no obvious correlation with sample thickness. The domain sizes of the surface layer in the 1000 and 500 μm

15 May 2025 04:16:25

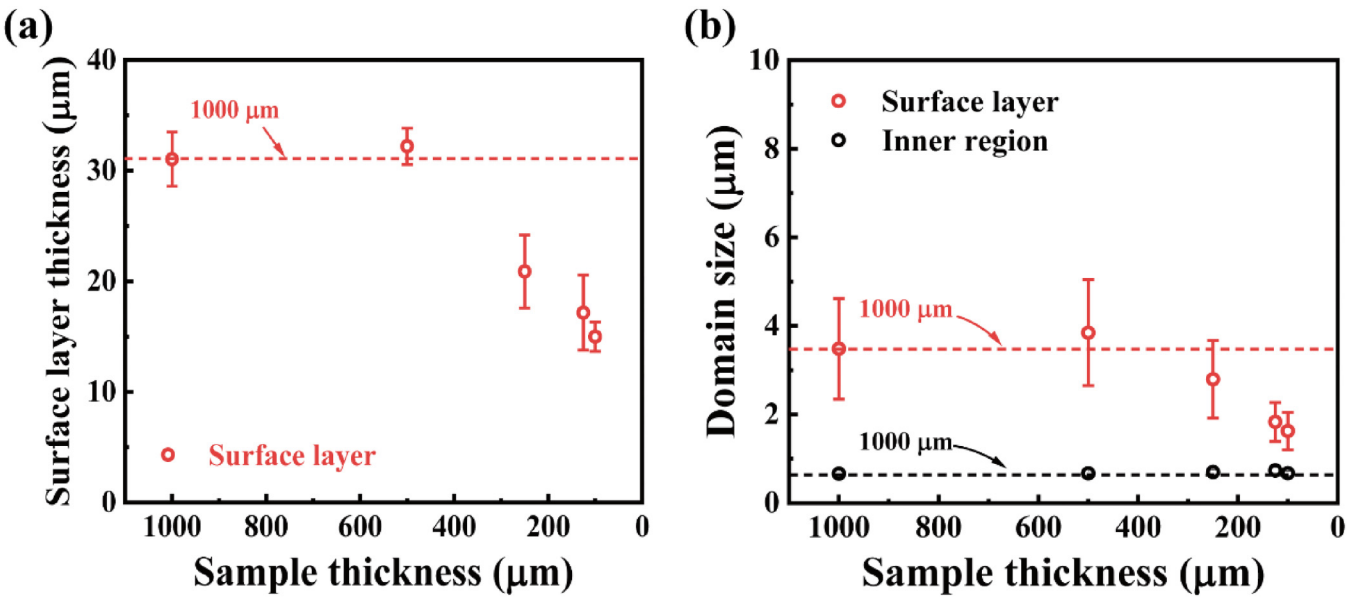

FIG. 3. Measured (a) surface layer thickness and (b) domain size in the surface layer and the inner region of AC-poled (50 cycles) PMN–28PT single crystal samples with thicknesses of 1000, 500, 250, 125, and 100 μm.

© Author(s) 2025

TABLE I. Measured domain size in the surface layer and the inner region and surface layer thickness of AC-poled (50 cycles) PMN–28PT single crystal samples with thicknesses of 1000, 500, 250, 125, and 100 μm.

Sample thickness (μm)	Domain size (μm)		Surface layer (μm)
	Inner region	Surface layer	
1000	0.66 (±0.05)	3.5 (±1.1)	31 (±2.5)
500	0.67 (±0.04)	3.9 (±1.2)	32 (±1.6)
250	0.70 (±0.05)	2.8 (±0.9)	21 (±3.3)
125	0.74 (±0.06)	1.8 (±0.4)	17 (±3.4)
100	0.67 (±0.05)	1.6 (±0.4)	15 (±1.3)

samples were greater than 3 μm [3.5 (±1.1) and 3.9 (±1.2) μm], while those in the 250, 125, and 100 μm samples were 2.8 (±0.9), 1.8 (±0.4), and 1.6 (±0.4) μm, respectively. As the distance from the surface increased, the size of large domains in the surface layer gradually decreased, eventually becoming similar to those in the inner region. These gradual variations in the domain size may contribute to an increase in the error bars for the average domain size in the surface layer. The surface layers in the 1000 and 500 μm samples were above 30 μm [31 (±2.5) and 32 (±1.6) μm], whereas those in the 250, 125, and 100 μm samples were 21 (±3.3), 17 (±3.4), and 15 (±1.3) μm, respectively. Both the surface layer thickness and its domain size decreased as the sample thickness decreased below 500 μm. Even though these decreased, the domain sizes in the surface layer remained more than twice as large as those in the inner region. Thus, the volume fraction of the surface layer increased as the sample thickness decreased. It indicates that the density of 109.5° domain wall decreases as the sample thickness decreases. In light of these aspects, the decreased ϵ_r and the increase in both E_c and tanδ of AC-poled single crystals as the sample thickness decreases can be attributed to the reduced density of 109.5° domain wall, which causes a reduction in the soft path. The decreased density of 109.5° domain wall can also reduce the P_r as the sample thickness decreases.

Figure 4 shows the dielectric properties of unpoled PMN–28PT single crystal samples with thicknesses of 1000, 500, 250, 125, and 100 μm. The unpoled samples show that the dielectric permittivity (ϵ_r), dielectric loss (tanδ), and phase angle (°) increase as the sample thickness decreases, except for the 250 μm thickness sample [i.e., it exhibits decreased dielectric permittivity (ϵ_r) and multiple peaks in dielectric loss (tanδ) and phase angle, and these anomalies were highly repeatable] as indicated in Fig. 4. It indicates that the surface layer deviates more from an ideal capacitor compared to the inner region, leading to an increase in conductive loss as the sample thickness decreases. The anomalies in dielectric properties of the unpoled 250 μm thickness sample may be related to the self-polarization phenomenon discovered in ferroelectric thin films[49–51] and single crystals grown using the solid-state crystal growth method.[52–55] This issue is beyond the scope of the present work and will be addressed in future research.

Figure 5(a) presents contour maps of the current as a function of the applied electric field and the number of AC-poling cycles,

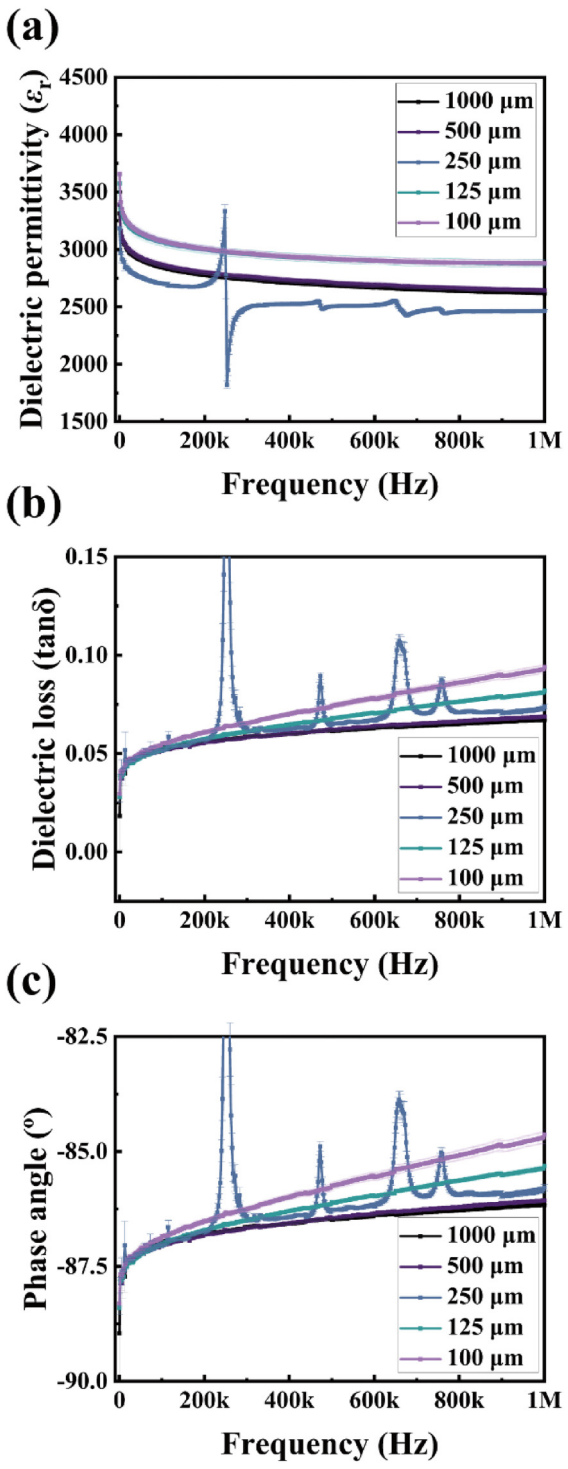

FIG. 4. (a) Dielectric permittivity (ϵ_r), (b) dielectric loss (tanδ), and (c) phase angle (°) of unpoled PMN–28PT single crystal samples with thicknesses of 1000, 500, 250, 125, and 100 μm.

15 May 2025 04:16:25

© Author(s) 2025

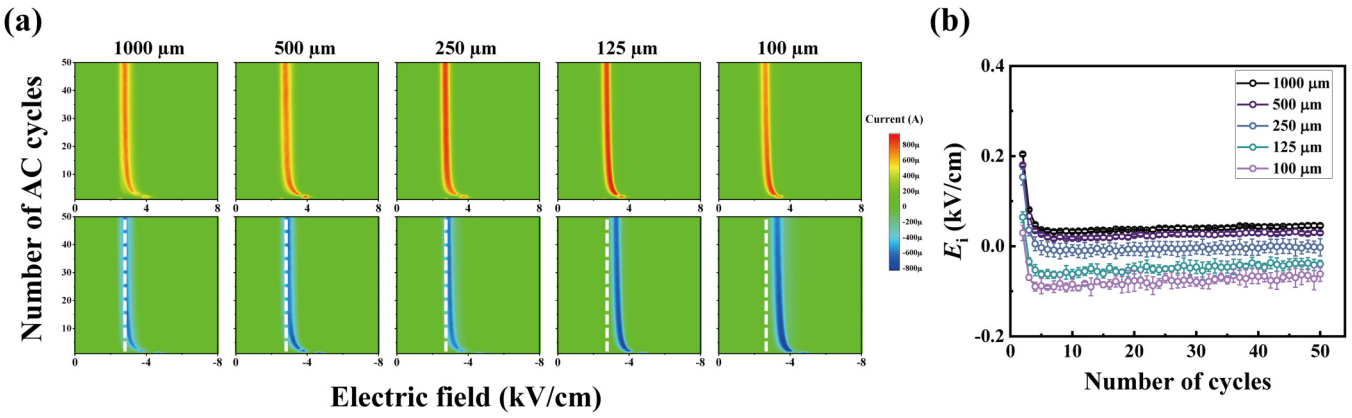

FIG. 5. (a) Contour maps showing the current as a function of the applied electric field and (b) internal bias field as a function of the number of AC-poling cycles for different thicknesses of PMN–28PT single crystal samples.

which were used to reconstruct P–E curves (see Fig. S4 in the supplementary material for intuitive understanding). It qualitatively demonstrates the difference in the electric field corresponding to the maximum and minimum polarization switching current peaks between the first half (positive electric field range) and the last half (negative electric field range) of each cycle. The internal bias (E_i) of samples was measured as a function of the number of AC-poling cycles using the P–E hysteresis loops (see Fig. S1 in the supplementary material) with changes in the sample thickness as shown in Fig. 5(b). The results clearly reveal two distinct behaviors: (1) A rapid decrease in E_i within the first five cycles irrespective of the sample thickness, and (2) a gradual increase in E_i toward more negative values as the sample thickness decreases. For the first five AC-poling cycles, the 70.5° domain walls rapidly decrease during each half cycle with polarization reversal induced by the electric field.[45] As the AC-poling cycle starts in the positive direction and ends in the negative direction, the negative coercive field ($-E_c$) is consistently smaller than the positive coercive field ($+E_c$) in the initial state. Therefore, the observed decrease in E_i during the first five cycles results from the rapid reduction in the density of 70.5° domain wall with each half cycle. The gradual increase in E_i toward negative values as the sample thickness decreases indicates that the domain becomes harder to reverse its polarization direction into the negative direction. It may be attributed to the fact that space charge can move more easily in the surface layer of the unpoled crystals and drifts during the first half of the AC-poling cycle due to the higher conductive loss of the surface layer compared to the inner layer. Subsequently, when the single crystal is polarized after the first half cycle, the space charge accumulated in the surface layer can no longer be easily released from the layer by applying an electric field due to the improved capacitance and reduced dielectric loss of the inner layer after the first half cycle. Genenko and

15 May 2025 04:16:25

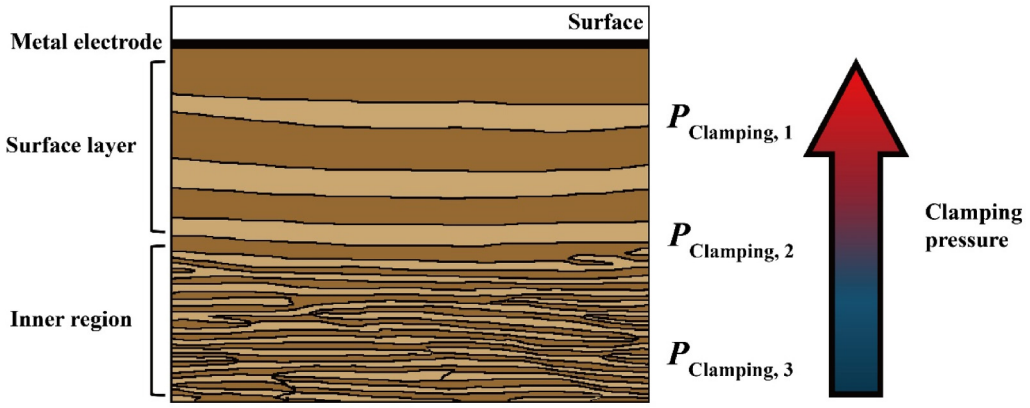

FIG. 6. Schematic illustration of the domain structure near the surface of AC-poled [001]-oriented PMN–28PT single crystal with the variation in clamping pressure depending on the distance from the surface.

© Author(s) 2025

Lupascu *et al.*[56–58] suggested that space charge in ferroelectric materials can induce clamping pressure at a domain wall, thereby preventing its switching through the drift mechanism. Therefore, the accumulated space charge in the surface layer can provide clamping pressure on the domain wall, hence stabilizing large domains within this layer. This suggests that the surface space charge plays a critical role in maintaining large domains in the surface layer of rhombohedral phase PMN–PT single crystals.

Figure 6 illustrates a schematic of the domain structure near the surface of the AC-poled PMN–28PT single crystal with the variation in clamping pressure depending on the distance from the surface. The clamping pressure gradually decreased as the distance from the surface increased and eventually approached zero as the distance became sufficiently large ($P_{\text{Clamping},1} > P_{\text{Clamping},2} > P_{\text{Clamping},3} \simeq 0$). As a result, the domain size gradually decreased with increasing distance from the surface due to the gradual decrease in the stabilizing clamping pressure required to maintain a large domain size.

CONCLUSION

In summary, the mechanism underlying the scaling effect that degrades the polarization and dielectric properties of the AC-poled [001]-oriented rhombohedral PMN–28PT single crystals was investigated. The coercive field (E_c) of crystals increased, whereas the remnant polarization (P_r) and dielectric properties of AC-poled samples degraded as the sample thickness decreased. It was observed that the domain structure of the AC-poled crystals consists of 109.5° domain walls, and the domain size in the surface layer was more than twice that of the inner region, irrespective of the sample thickness. Although the thickness of the surface layer and its domain size decreased, its volume fraction increased as the sample thickness decreased. Therefore, we propose that the scaling effects in the AC-poled [001]-oriented rhombohedral PMN–PT single crystals can be attributed to a decrease in the density of 109.5° domain wall in the surface layer. The accumulated space charge in the surface induced internal bias field (E_i), and it is considered the reason for stabilizing the large domains in the surface layer. These results may contribute to addressing the scaling effect issues in high-performance transducers for high-frequency ultrasound biomicroscope applications.

SUPPLEMENTARY MATERIAL

See the supplementary material for the details of the electric field-dependent polarization results used for calculating the coercive field and remnant polarization, and the schematic illustration demonstrating how the contour maps were plotted.

ACKNOWLEDGMENTS

This research was supported by the Material Technology Development Program (No. 2410004461) through the Korea Evaluation Institute of Industrial Technology (KEIT).

AUTHOR DECLARATIONS

Conflict of Interest

The authors have no conflicts to disclose.

Author Contributions

Woo-Jin Choi: Conceptualization (equal); Data curation (lead); Formal analysis (lead); Methodology (equal); Writing – original draft (lead); Writing – review & editing (equal). **Hye-Lim Yu:** Conceptualization (equal); Methodology (equal); Writing – review & editing (equal). **Jeong-Woo Sun:** Data curation (supporting); Writing – review & editing (supporting). **Sang-Goo Lee:** Funding acquisition (equal); Methodology (equal); Resources (equal). **Yoon-Sang Jeong:** Methodology (equal); Resources (equal). **Wook Jo:** Conceptualization (equal); Supervision (lead); Writing – review & editing (lead).

DATA AVAILABILITY

The data that support the findings of this study are available within the article.

REFERENCES

[1]B. Jaffe, W. R. Cook, and H. Jaffe, *Piezoelectric Ceramics* (Academic, New York, 1971).
[2]K. Uchino, *Advanced Piezoelectric* Materials: Science and Technology (Woodhead Publishing, Cambridge, 2017).
[3]J. Chen and R. Panda, in *IEEE International Ultrasonic Symposium* (IEEE, 2005), p. 235.
[4]X. M. Lu and T. Proulx, in *IEEE International Ultrasonic Symposium* (IEEE, 2005), p. 227.
[5]Y. Hosono and Y. Yamashita, J. Electroceram. **17**, 577 (2006).
[6]Y. Yamashita, T. Karaki, H.-Y. Lee, H. Wan, H.-P. Kim, and X. Jiang, IEEE Trans. Ultrason. Ferroelectr. Freq. Control **69**, 3048 (2022).
[7]A. B. Kounga, T. Granzow, E. Aulbach, M. Hinterstein, and J. Rödel, J. Appl. Phys. **104**, 024116 (2008).
[8]B. Li, J. E. Blendell, and K. J. Bowman, J. Am. Ceram. Soc. **94**, 3192 (2011).
[9]L. Gimadeeva, Q. Hu, X. Wei, D. Alikin, and V. Y. Shur, Ferroelectrics **605**, 36 (2023).
[10]M. Rotan, M. Zhuk, and J. Glaum, J. Euro. Ceram. Soc. **40**, 5402 (2020).
[11]H. Wang, J. Liu, S. Sadeghzade, R. Hou, and H. Yuan, Ceram. Int. **49**, 11334 (2023).
[12]J.-W. Sun, W.-J. Choi, H.-L. Yu, S.-G. Lee, J. E. Ryu, T. T. Zate, and W. Jo, J. Kor. Ceram. Soc. **61**, 854 (2024).
[13]A. Kounganjiwa, E. Aulbach, T. Granzow, and J. Rödel, Acta Mater. **55**, 675 (2007).
[14]J. Rödel, A. B. Kounga, E. Aulbach, T. Granzow, and T. Leist, in *2007 6th IEEE International Symposium on the Applications of Ferroelectrics* (IEEE, 2007), p. 638.
[15]Y.Y. N. Yamamoto, Y. Hosono, K. Itsumi, and K. Higuchi, U.S. patent 0062261 A1 (6 March 2014).
[16]N.Y. Y. Yamashita, Y. Hosono, and K. Itsumi, U.S. patent 0372219 A1 (24 December 2015).
[17]D. Ren, C. Li, J. Shi, and R. Chen, IEEE Trans. Ultrason. Ferroelectr. Freq. Control **69**, 1848 (2021).
[18]Y. Guan, H. Hang, D. Lin, X. a. Wang, Y. Tang, and H. Luo, Sens. Actuators A: Phys. **354**, 114275 (2023).
[19]D. Weiyan, X. Chen, Y. Zhang, X. Li, F. Sun, Z. Yang, X. Tang, C. Zhou, F. Wang, and X. Zhao, Ultrason. Imaging **46**, 312 (2024).
[20]X. Bai, D. Wang, L. Zhen, M. Cui, J. Liu, N. Zhao, C. Lee, and B. Yang, Int. J. Extreme Manuf. **6**, 062001 (2024).
[21]R. H. Silverman, Clin. Exp. Ophthalm. **37**, 54 (2009).
[22]M. He, D. Wang, and Y. Jiang, J. Curr. Glaucoma Pract. **6**, 25 (2012).
[23]K. K. Shung, J. Cannata, and Q. Zhou, J. Electroceram. **19**, 141 (2007).
[24]S. Zhang and F. Li, J. Appl. Phys. **111**, 031301 (2012).
[25]Z. Yang and J. Zu, Energy Convers. Manag. **122**, 321 (2016).

15 May 2025 04:16:25

© Author(s) 2025

[26]J. Erhart, P. Půlpán, and M. Pustka, *Piezoelectric Ceramic Resonators* (Springer, New York, 2017).
[27]T. Namba, A. Tanaka, T. Sato, and Y. Sakano, Jpn. J. Appl. Phys. **62**, SM1016 (2023).
[28]H. Dammak, M. Guennou, C. Ketchazo, M. P. Thi, F. Brochin, T. Delaunay, P. Gaucher, E. Le Clezio, and G. Feuillard, in *15th IEEE International Symposium on the Applications of Ferroelectrics* (IEEE, 2006), p. 249.
[29]H. J. Lee, S. Zhang, and T. R. Shrout, J. Appl. Phys. **107**, 124107 (2010).
[30]H. J. Lee, S. Zhang, J. Luo, F. Li, and T. R. Shrout, Adv. Funct. Mater. **20**, 3154 (2010).
[31]L. Li, X. Zhao, X. Li, Q. Xu, L. Yang, S. Wang, and H. Luo, J. Appl. Phys. **115**, 204104 (2014).
[32]H. Takahashi, H. Suzuki, and Y. Namba, CIRP Ann. **65**, 541 (2016).
[33]C. Luo, H. Wan, W.-Y. Chang, Y. Yamashita, A. R. Paterson, J. Jones, and X. Jiang, Appl. Phys. Lett. **115**, 192904 (2019).
[34]C. Qiu, J. Liu, F. Li, and Z. Xu, J. Appl. Phys. **125**, 014102 (2019).
[35]D. Tian, P. Chen, X. Yang, and B. Chu, Ceram. Int. **47**, 17262 (2021).
[36]J. Xiong, Z. Wang, X. Yang, R. Su, X. Long, and C. He, Phys. Status Solidi B **259**, 2100287 (2022).
[37]H.-P. Kim, H. Wan, X. Lu, Y. J. Yamashita, and X. Jiang, Appl. Phys. Lett. **120**, 142901 (2022).
[38]L. Ning, C. Wang, N. Jia, Z. Ma, Y. Dang, C. Sun, H. Du, Z. Xu, and F. Li, Appl. Phys. Lett. **124**, 262902 (2024).
[39]M. Budimir, D. Damjanovic, and N. Setter, J. Appl. Phys. **94**, 6753 (2003).
[40]M. Budimir, D. Damjanovic, and N. Setter, Phys. Rev. B **72**, 064107 (2005).
[41]M. Budimir, D. Damjanovic, and N. Setter, Phys. Rev. B **73**, 174106 (2006).
[42]B. Wang, F. Li, and L. Q. Chen, Adv. Mater. **33**, 2105071 (2021).
[43]K. Baba-Kishi, G. Pang, C. Choy, H. Chan, H. Luo, Q. Yin, and Z. Yin, Ferroelectrics **253**, 55 (2001).
[44]T. Liu and C. S. Lynch, Smart Mater. Struct. **5053**, 347 (2003).
[45]H. Wan, C. Luo, C. Liu, W.-Y. Chang, Y. Yamashita, and X. Jiang, Acta Mater. **208**, 116759 (2021).
[46]J. Fan, X. Lu, and W. Cao, J. Alloys Compd. **835**, 155171 (2020).
[47]C. Qiu, B. Wang, N. Zhang, S. Zhang, J. Liu, D. Walker, Y. Wang, H. Tian, T. R. Shrout, Z. Xu, L.-Q. Chen, and F. Li, Nature **577**, 350 (2020).
[48]H. P. Kim, H. Wan, C. Luo, Y. Sun, Y. Yamashita, T. Karaki, H. Y. Lee, and X. Jiang, IEEE Trans. Ultrason. Ferroelectr. Freq. Control **69**, 3037 (2022).
[49]A. L. Kholkin, K. G. Brooks, D. V. Taylor, S. Hiboux, and N. Setter, Integr. Ferroelectr. **22**, 525 (1998).
[50]V. P. Afanasjev, A. A. Petrov, I. P. Pronin, E. A. Tarakanov, E. J. Kaptelov, and J. Graul, J. Phys.: Condens. Matter **13**, 8755 (2001).
[51]Z. Kighelman, D. Damjanovic, and N. Setter, J. Appl. Phys. **89**, 1393 (2001).
[52]C. He, Z. Wang, X. Li, X. Yang, X. Long, and Z.-G. Ye, Acta Mater. **125**, 498 (2017).
[53]H. Maiwa, Y. Yamagata, Y. Xiang, H.-Y. Lee, and Y. Yamashita, Jpn. J. Appl. Phys. **63**, 10SP01 (2024).
[54]H. Maiwa, Y. Yamagata, Y. Xiang, H. Sun, H.-Y. Lee, and Y. Yamashita, Jpn. J. Appl. Phys. **63**, 04SP50 (2024).
[55]H.-P. Kim, G.-J. Lee, J.-H. Lee, J.-H. Cho, H.-L. Yu, W.-S. Kang, J.-H. Kang, H.-Y. Lee, and W. Jo, J. Materiomics **11**, 100887 (2025).
[56]D. C. Lupascu, Y. A. Genenko, and N. Balke, J. Am. Ceram. Soc. **89**, 224 (2006).
[57]Y. A. Genenko and D. C. Lupascu, Phys. Rev. B **75**, 184107 (2007).
[58]Y. A. Genenko, N. Balke, and D. C. Lupascu, Ferroelectrics **370**, 196 (2008).

15 May 2025 04:16:25

© Author(s) 2025